THE JOURNAL OF
PHYSICAL CHEMISTRY A

ARTICLE

pubs.acs.org/JPCA

Effects of Excitation Energy on the Autodetachment Lifetimes of Small Iodide-Doped ROH Clusters ($R{=}H-$, CH_3-, CH_3CH_2-)

Margaret A. Yandell,[†] Ryan M. Young,[†] Sarah B. King,[†] and Daniel M. Neumark*[,†,‡]

[†]Department of Chemistry, University of California, Berkeley, California 94720, United States

[‡]Chemical Sciences Division, Lawrence Berkeley National Laboratory, Berkeley, California 94720, United States

S *Supporting Information*

ABSTRACT: The effect of excitation energy on the lifetimes of the charge-transfer-to-solvent (CTTS) states of small ($4 \leq n \leq 10$) iodide-doped water and alcohol clusters was explored using femtosecond time-resolved photoelectron imaging. Excitation of the CTTS state at wavelengths ranging from 272 to 238 nm leads to the formation of the $I\cdots(ROH)_n^-$ ($R{=}H-$, CH_3-, and CH_3CH_2-) species, which can be thought of as a vibrationally excited bare solvent cluster anion perturbed by an iodine atom. Autodetachment lifetimes for alcohol-containing clusters range from 1 to 71 ps, while water clusters survive for hundreds of ps in this size range. Autodetachment lifetimes were observed to decrease significantly with increasing excitation energy for a particular number and type of solvent molecules. The application of Klots' model for thermionic emission from clusters to $I^-(H_2O)_5$ and $I^-(CH_3OH)_7$ qualitatively reproduces experimental trends and reveals a high sensitivity to energy parametrization while remaining relatively insensitive to the number of vibrational modes. Experimental and computational results therefore suggest that the rate of electron emission is primarily determined by the energetics of the cluster system rather than by details of molecular structure.

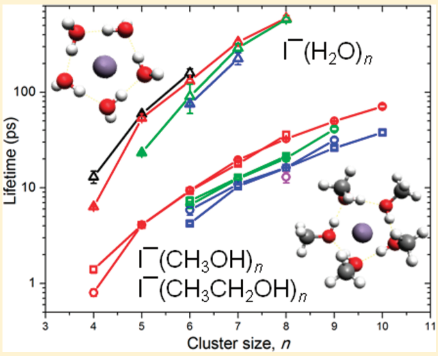

INTRODUCTION

Charge stabilization by bulk and local solvent environments has been a major focus of study in recent years in part due to the interest surrounding solvated electron phenomena in chemical, physical, and biological research communities.[1,2] While electron solvation is generally considered a "bulk" phenomenon, gas phase cluster studies of excess electrons bound to a known number of solvent molecules have provided significant insights into electron binding motifs and the fundamental processes associated with the formation and accommodation of a solvated charge.[3−5] These studies have been complemented by experiments on halide−solvent clusters in which the excess electron on the halide is ejected onto the solvent network via excitation of the cluster analog of the charge-transfer-to-solvent (CTTS) band in the ultraviolet[6] producing, after some dynamics, a solvated electron and providing a direct comparison to the analogous process in bulk solvents.[7] Cluster dynamics studies performed to date have focused on femtosecond time-resolved experiments on an iodide anion bound to water,[8,9] methanol,[10] and other solvating species.[11−13] These studies show a strong dependence of the electron solvation dynamics on the size and composition of the cluster, and that the CTTS excited state in iodide−water and iodide−methanol clusters decays by autodetachment to a neutral cluster and a free electron. In this paper, we focus on this decay mechanism in more detail and investigate the autodetachment dynamics subsequent to CTTS excitation over a range of excitation energies in $I^-(H_2O)_n$, $I^-(CH_3OH)_n$, and $I^-(CH_3CH_2OH)_n$ clusters. We also examine whether the autodetachment rates and associated electron kinetic energy distributions can be accurately described by statistical models.

Previous work on charge-transfer-to-solvent dynamics in iodide-doped water and methanol clusters revealed notable differences between the electron solvation processes in the two species. Time-resolved photoelectron spectra for iodide−water clusters suggested that upon excitation of the CTTS band the excess electron was first promoted to a diffuse state near the iodine atom before solvent rearrangement leading to stabilization over a few picoseconds.[9] After tens of ps, the vertical detachment energy (VDE), a measure of electron binding strength, was observed to decrease slightly as the iodine atom departed the cluster.[9,14] The lifetime of the CTTS state ranged from approximately 0.6−3000 ps for $n = 3-10$ with excitation at 4.65 eV (267 nm). The decay of this state was mirrored by the recovery of a second spectral feature near zero electron kinetic energy attributed to electron autodetachment. This feature was also present in single-photon UV spectra, suggesting that it is the ultimate decay mechanism for the CTTS state.[9]

Photoelectron spectra of iodide-doped methanol clusters also revealed autodetachment and pump−probe features with

Special Issue: Femto10: The Madrid Conference on Femtochemistry

Received: August 19, 2011
Revised: October 10, 2011
Published: November 01, 2011

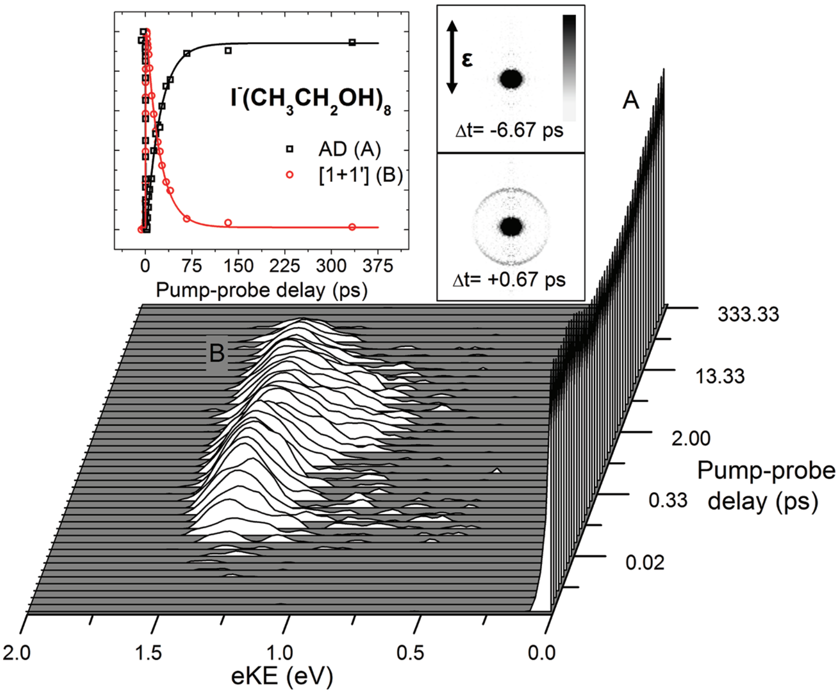

Figure 1. Time-resolved photoelectron spectrum for $I^-(CH_3CH_2OH)_8$ with excitation energy = 4.85 eV (256 nm). Electron kinetic energy (eKE) increases from right to left, while pump–probe delay increases from front to back. The intensity of the peak near zero eKE, "A", is scaled by 0.1 for ease of viewing. The inset in the upper left corner shows the normalized integrated intensities of "A" (autodetachment, AD) and "B" (resonant pump–probe signal, [1 + 1′]). The inset at right shows the evolution of these features with pump–probe delay in processed images. The vertical arrow indicates the laser polarization while the gradient indicates the feature's intensity.

near-identical time constants, but the iodide–methanol CTTS state lifetimes were much shorter, ranging from 0.8 to 86 ps for $n = 4-11$ with excitation at 4.71 eV (263 nm).[10] This difference was attributed to the instability of bare methanol cluster anions in this size range with respect to electron loss.[15] As in water, the ejected electron in the methanol-containing clusters is thought to first occupy a diffuse state near the iodine atom before solvent rearrangement leads to an initial stabilization. This stabilization is short-lived, however, as both the VDE and the width of the CTTS spectral feature were observed to evolve dramatically before the decay of the CTTS state by autodetachment. These dynamics were suggested to result from a concerted rotation of one or more methanol molecules to enhance the cluster's hydrogen bonding network.[10] Ethanol has the same hydrogen bonding capability as methanol but more vibrational modes, raising the question of how the CTTS dynamics of $I^-(\text{ethanol})_n$ and $I^-(\text{methanol})_n$ clusters would compare.

Studies of charge-transfer-to-solvent dynamics in iodide-doped water and methanol clusters have previously involved the use of a single excitation energy to promote the charge transfer onto the solvent network. CTTS bands blue-shift to the deep UV (219–230 nm for ethanol, methanol, and water)[16−18] with increasing cluster size as n increases.[7] The resonance of the CTTS transition is therefore size-dependent. While the studies of Verlet et al. and Kammrath et al. of $I^-(H_2O)_n$ clusters[8,9] and that by Ehrler et al. of $I^-(CH_3CN)_n$ clusters[13] utilized different photon energies to access the CTTS band in different size ranges, no study yet presented has investigated the effect of pumping different regions of the CTTS band for a cluster of a particular size.

To better understand dynamics in iodide–solvent clusters following CTTS excitation, we have investigated for the first time the effects of excitation energy on autodetachment lifetimes for small ($4 \leq n \leq 10$) iodide-doped ethanol, methanol, and water clusters as a function of solvent type and cluster size. We have also applied Klots' microcanonical formalism for thermionic emission to model observed trends.[19] Autodetachment lifetimes were determined to increase with cluster size and decrease with excitation energy. Lifetimes for methanol- and ethanol-containing clusters were nearly identical for the same excitation energy and number of molecules and were significantly smaller than those observed for iodide-doped water clusters. We find that the Klots model effectively recovers these differences from approximate vibrational frequencies and appropriate energy parametrization and that it reproduces the form of the low kinetic energy photoelectron signal resulting from autodetachment. The high sensitivity of modeling results to energetics and the low sensitivity of experimental results to the number of vibrational modes implies that the energetics of the various cluster systems are more important in determining their excited state lifetimes than the precise structural identities of the molecules therein.

■ EXPERIMENTAL SECTION

Details of the femtosecond time-resolved photoelectron imaging experiment have been described elsewhere.[20,21] Argon gas at 5–20 psig was flowed over reservoirs of ROH (R═H–, CH_3–, CH_3CH_2–) and methyl iodide and expanded through an Even-Lavie valve pulsed at 100 Hz.[22] The solvent reservoir and gas line were heated slightly for effective $I^-(\text{ethanol})_n$ production. The pulsed beam was then passed through a ring-shaped ionizer to generate cluster anions via secondary electron attachment before their perpendicular extraction with a Wiley–McLaren time-of-flight mass spectrometer.[23] Clusters of the desired mass were isolated with a pulsed electrostatic switch before entering the interaction region where they were intercepted by femtosecond pump and probe laser pulses. The resulting photoelectrons were then collinearly accelerated via velocity map imaging[24] to a pair of chevron-mounted microchannel plates coupled to a phosphor screen. Images from the phosphor screen were captured with a charge-coupled device camera and reconstructed using the basis-set expansion method (BASEX)[25] following four-way symmetrization to address detector inhomogeneities. The reconstructed images provided both electron kinetic energy and photoelectron angular distributions (PADs). Anisotropy parameters, β_i, describing the detached electron's angular momentum, were obtained by fitting PADs to an even series of Legendre polynomials:[26,27]

$$I(\theta) = \frac{\sigma_{\text{total}}}{4\pi}[1 + \beta_2 P_2(\cos\theta) + \beta_4 P_4(\cos\theta)] \qquad (1)$$

where I represents intensity, θ the angle between the laser polarization and the ejected electron, and σ_{total} the total photodetachment cross section. One-photon detachment is described with a single anisotropy parameter, β_2, while two-photon detachment requires an additional parameter.

Femtosecond pump and probe laser pulses were generated with a Ti:sapphire oscillator and multipass amplifier (KM Laboratories Griffin Oscillator and Dragon Amplifier). The resulting 790 nm pulses were approximately 35 fs in duration and ∼2 mJ/pulse at a 600 Hz repetition rate. Most of this light was used to generate a UV pump pulse either with a third-harmonic generator to produce 263 nm light (∼20 μJ/pulse) or by second harmonic generation of the sum frequency of the fundamental and the high or low frequency output of an optical parametric amplifier (Light Conversion TOPAS-C) to produce 238−272 nm (∼10 μJ/pulse) tunable UV light. The remainder of the fundamental was used as the probe pulse (∼150 μJ/pulse). Cross-correlation measurements taken at the entrance to the vacuum chamber reveal pulse widths ranging from 80 to 200 fs.

■ RESULTS

Time-resolved photoelectron imaging was used to investigate the effects of changing excitation energy on CTTS dynamics in iodide-doped ethanol, methanol, and water clusters of four to ten molecules. Figure 1 displays reconstructed images, normalized integrated intensities, and photoelectron spectra for $I^-(\text{ethanol})_8$, which are typical for the size range studied here. Electron kinetic energy is shown increasing from right to left with pump−probe delay increasing from front to back. Two features are evident in the spectra and images: a peak with near zero electron kinetic energy (scaled by 0.1 in the figure for clarity) labeled "A" and a peak near 1.5 eV denoted "B" that emerges at positive pump−probe delays. At 263 nm, "A" dominates the spectra for the smallest cluster size and decreases in relative intensity as n increases and the charge-transfer-to-solvent band blue shifts. Similar trends are observed with higher excitation energies. The images in the inset reveal that "A" is isotropic, while the intensity of "B" is maximized parallel to the laser polarization.

For all cluster sizes and excitation energies, the integrated intensities of "A" and "B" demonstrate complementary time dependence (Figure 1). The population of "A" is relatively constant for negative and very positive pump−probe delays. When the pump−probe delay is near zero, the intensity of "A" decreases sharply as "B" appears. The two features return to their initial values in an exponential fashion.

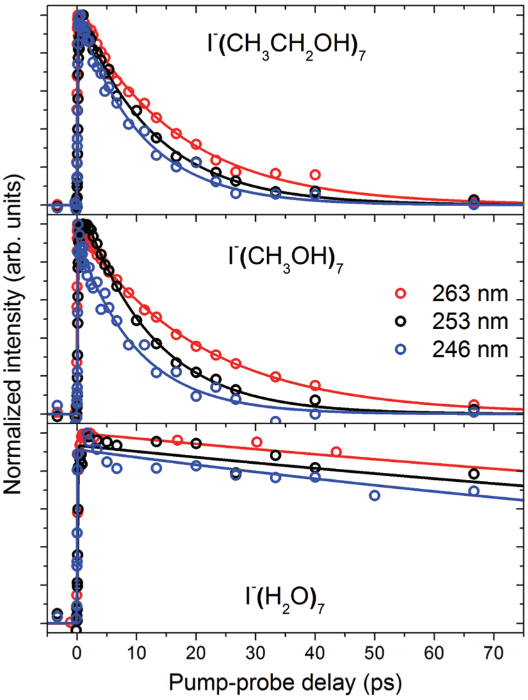

Figure 2. Normalized integrated intensities for "B" of iodide-doped clusters of seven molecules of ethanol (upper panel), methanol (middle panel), and water (bottom panel) with excitation energies of 263 (red), 253 (black), and 246 nm (blue). Lines between points are fits described in the Analysis section.

The spectral features and trends described for $I^-(\text{ethanol})_n$ clusters are similar to those observed for $I^-(\text{water})_n$ and $I^-(\text{methanol})_n$ clusters and were observed here for all solvent identities, cluster sizes, and excitation energies sampled.[9,10] The evolution of the peak center and width of the CTTS spectral feature with pump−probe delay is also similar for iodide-doped ethanol and methanol clusters. Based on the similarities between these results and previous work, "A" is attributed to vibrational autodetachment of the pump-excited cluster anion, while "B" is assigned to resonant pump−probe detachment via the CTTS state. The two decay channel model implied by these assignments explains the similar time-dependence of the two features: the excited CTTS state must either undergo autodetachment or experience photodetachment by the probe pulse.[9,10,13]

Figure 2 displays the normalized integrated intensities of the CTTS feature excited at various pump energies for iodide-doped ethanol, methanol, and water clusters containing seven solvent molecules. The CTTS excited states of ethanol- and methanol-containing clusters reveal similar time-dependent behavior while that for water-containing clusters appears much longer lived. The lifetimes of the excited state feature appear to decrease as the excitation energy increases for all solvents. These trends are observed for all cluster sizes, n.

■ ANALYSIS

The complementary time dependence exhibited by the autodetachment and CTTS features for each cluster solvent, size, and excitation energy studied can be analyzed after extraction of integrated intensities at each pump−probe delay. Population

Table 1. Lifetimes of Iodide-Doped Solvent Clusters at Various Excitation Energies

	$I^-(CH_3OH)_n$				$I^-(CH_3CH_2OH)_n$		
n	263 nm[a]	255 nm	245 nm	238 nm	263 nm	255 nm	245 nm
4	0.8 ± 0.1				1.4 ± 0.1		
5	4.1 ± 0.0				4.1 ± 0.2		
6	9.4 ± 0.5	6.6 ± 0.6	5.9 ± 0.7		9.3 ± 0.1	7.3 ± 0.7	4.2 ± 0.2
7	19.6 ± 0.5	12.4 ± 0.5	10.9 ± 0.7		17.8 ± 0.5	12.7 ± 0.5	10.4 ± 0.4
8	32.6 ± 0.4	20.4 ± 1.4	16.3 ± 1.1	13.0 ± 1.7	36.0 ± 3.1	21.5 ± 0.5	16.2 ± 0.2
9	49.7 ± 0.8	41.2 ± 2.1	31.6 ± 2.0				26.1 ± 1.1
10	70.9 ± 2.6						37.9 ± 2.1

	$I^-(H_2O)_n$			
n	272 nm	263 nm[b]	255 nm	245 nm
4	13.0 ± 1.9	6.4 ± 0.1		
5	59.4 ± 2.2	53.6 ± 1.9	23.2 ± 0.3	
6	159.1 ± 16.5	131.3 ± 4.6	90.4 ± 30.7	75.6 ± 2.1
7		334.7 ± 11.5	290.2 ± 31.3	225.2 ± 32.0
8		594.6 ± 37.0	579.9 ± 29.5	

[a] Young et al. 2011.[10] [b] Kammrath et al. 2005.[9] See text for details on fitting.

dynamics are modeled with single or biexponential decay; for $t \geq t_0$, where t_0 is the zero of pump−probe delay, the multiexponential function is convoluted with a Gaussian function to account for experimental response. A delta function centered at t_0 accounts for coherence artifacts during the period of cross-correlation of the pump and probe pulses while an offset, I_0, addresses background:[10]

$$I = e^{-t^2/\sigma^2} * \begin{cases} I_0, & t < t_0 \\ I_0 + a_0\delta(t - t_0) + \sum_i a_i \exp\left[-\left(\frac{t - t_0}{\tau_{X_i}}\right)\right], & t \geq t_0 \end{cases} \tag{2}$$

In eq 2, σ represents the temporal width of the Gaussian function and X is either A or B (CTTS). In general, the smallest clusters (i.e., $n = 4, 5$) exhibit single exponential decay from t_0 ($i = 1$), while larger clusters ($n > 5$) achieve their maxima after t_0 before beginning to decay ($i = 2$). The rise time τ_{B1} for clusters following a biexponential pattern is approximately 1 ps for all materials studied. Time constants for "A" and "B" are generally within error bars of each other, with those for "A" often larger due to the inherent difficulty in measuring small changes over a large background. Thus, lifetimes presented in Table 1 and graphically summarized in Figure 3 are time constants τ_{B1} for processes described by single exponential decay and τ_{B2} for biexponential decay processes. These lifetimes increase with cluster size and decrease with excitation energy for each system. Varying the source backing pressure between 5 and 20 psig did not noticeably affect lifetime measurements.

It should be noted that lifetimes presented for $I^-(\text{water})_n$ at 263 nm were obtained using the fit function described here with data taken previously in our research group. The values reported by Kammrath et al.[9] were measured by first fitting the signal at each pump−probe delay to a Gaussian function and then applying a multiexponential fit to the calculated peak centers, neglecting values less than the maximum. The refitted lifetimes fall approximately within error bars of those previously reported for $n = 4$−7; for $n = 8$, the lifetime differs more significantly as

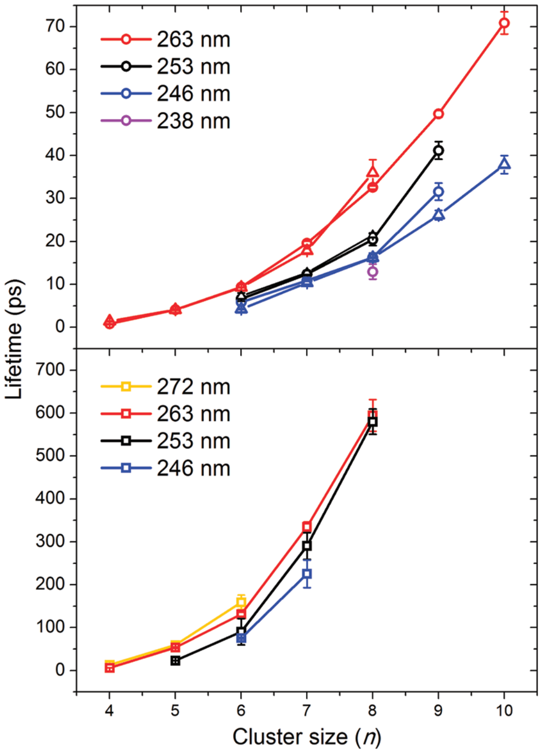

Figure 3. Top panel: Lifetimes of $I^-(CH_3OH)_n$ (circles) and $I^-(CH_3CH_2OH)_n$ clusters (triangles). Bottom panel: Lifetimes of $I^-(H_2O)_n$ (squares) clusters. Lifetimes presented are measured with excitation energies of 272 (orange), 263 (red), 253 (black), 246 (blue), and 238 (purple) nm. Wavelengths used are known to within ±2 nm. Lifetimes for $I^-(CH_3OH)_n$ at 263 nm are taken from Young et al.,[10] and lifetimes for $I^-(H_2O)_n$ at 263 nm are taken from spectra measured by Kammrath et al.,[9] as described in the text.

the decay is now treated with the convolution of a Gaussian and a multiexponential function where biexponential character captures a late rise to a maximum followed by decay rather than a complex decay from a maximum intensity.

■ DISCUSSION

The results in Table 1 and Figure 3 show that, for all solvent molecules and cluster sizes studied here, the excited state lifetime at fixed wavelength increases with cluster size but, for a fixed cluster size, decreases with increasing excitation energy. For all clusters, the longest and shortest lifetimes differ by about a factor of 2 over the range of wavelengths used here (272−238 nm). The other notable trend is that, at a given excitation wavelength, the lifetimes for $I^-(H_2O)_n$ clusters are considerably longer than for comparably sized $I^-(CH_3OH)_n$ and $I^-(CH_3CH_2OH)_n$ clusters, while clusters with the same number of CH_3OH and CH_3CH_2OH solvent molecules have essentially the same excited state lifetimes. For example, the lifetimes of $I^-(\text{methanol})_8$ and $I^-(\text{ethanol})_8$ at 263 nm excitation are 33 and 36 ps, respectively, but that for $I^-(\text{water})_8$ is 595 ps.

As discussed in previous work, the excited states in these halide-clusters are accessed by the cluster analog of CTTS transitions.[6,10] The complementary dynamics of "A" and "B" in the time-resolved photoelectron images show that these states decay by autodetachment. Hence, the overall autodetachment mechanism is

$$I^-(ROH)_n \xrightarrow{h\nu_{\text{pump}}} I\cdots(ROH)_n^- \xrightarrow{\tau_B} I\cdots(ROH)_n + e^- \qquad (3)$$

Given the large number of vibrational modes in these clusters and the very low energies of the electrons ejected by autodetachment, it is reasonable to see if these results can be understood within the framework of cluster thermionic emission. This is a statistical decay process that can be treated assuming either a canonical or microcanonical ensemble of clusters.[28] The microcanonical model developed by Klots[19] has previously been successfully applied to neutral and negatively charged clusters[29,30] and thus provides a useful framework within which we would like to explain the qualitative and quantitative trends seen here for halide-solvent clusters.

In this model, the rate of electron emission $k(E)$ is given by

$$k(E) = \frac{W(E, E_b)}{h\rho(E)} \qquad (4)$$

where h is Planck's constant, E is the total energy, E_b is the adiabatic binding energy, $W(E,E_b)$ is the total number of neutral states, and $\rho(E)$ is the density of anion states. The totality of neutral states and density of anion states should both increase dramatically with increasing energy. Each of these quantities should also be strongly dependent on the number of vibrational modes in the species of interest as they express the partitioning of energy among states with energy $\leq (E - E_b)$ for $W(E, E_b)$ and between (E and $E + dE$) for $\rho(E)$.

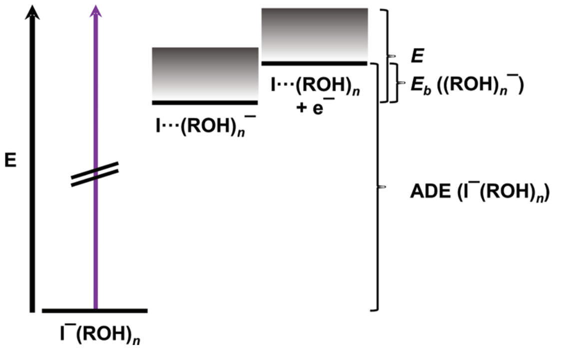

Figure 4. Schematic describing the energetics considered in the microcanonical rate theory modeling. The purple vertical arrow represents the excitation utilized to promote the charge-transfer-to-solvent transition. Gradients represent the densities of states of the anion and neutral species.

Equation 4 is similar to the RRKM expression for unimolecular dissociation,[31] but the numerator in eq 4 refers to the total number of available product states as opposed to the total number of states at the unimolecular transition state. The expressions are essentially equivalent in the limit of a transition state at infinite fragment separation, with the caveat that the number of nuclear degrees of freedom considered in the numerator and denominator of eq 4 is the same. Hence, some of the trends seen here are readily understood based on well-known results from RRKM theory. In particular, the increasing autodetachment rate with excitation energy and the decreasing rate with cluster size are characteristic of statistical decay models.

On the other hand, the dependence of the autodetachment rate on solvent is less intuitive. For a given cluster size, one might have expected the autodetachment rate to be considerably faster for $I^-(H_2O)_n$ than for the corresponding $I^-(CH_3OH)_n$ or $I^-(CH_3CH_2OH)_n$ cluster since the density of states at a particular excitation energy (i.e., the denominator in eq 4) is much smaller for iodide−water clusters. Instead, we find considerably slower autodetachment for water and about the same rate for methanol and ethanol clusters.

We therefore must carefully consider the energetics involved in eq 4 and determine how these differ for water- and methanol-/ethanol-containing clusters. With respect to eq 3, E is the excess energy of the $I\cdots(ROH)_n^-$ intermediate created by the pump pulse, and E_b is the adiabatic detachment energy (ADE) of this intermediate relative to the $I\cdots(ROH)_n + e^-$ products, as indicated in Figure 4. The binding energy of the iodine atom to the intermediate is estimated to be ~50 meV for water-containing clusters,[9,32,33] and if that is neglected, then E_b is the adiabatic electron binding energy of the $(ROH)_n^-$ cluster.[34] Given that small water cluster anions are readily seen in mass spectrometry[3,35] but methanol cluster anions are not observed until $n \sim 70$,[15] it is reasonable to assume that E_b is positive for water cluster anions but negative or only slightly positive for methanol (and presumably ethanol) cluster anions. This effect is the most likely origin for the slower autodetachment rates in water as it will significantly reduce the number of accessible product states (i.e., $W(E, E_b)$ in eq 4) for iodide−water clusters compared to the other solvent species.

To explore these effects more quantitatively, we need to explicitly evaluate the quantities in eq 4. For microcanonical thermionic emission,[19] the numerator is related to the kinetic energy distribution of the ejected electrons, $\rho(\varepsilon)$, by

$$W(E, E_b) = \int_0^{E - E_b} \rho(\varepsilon)\, d\varepsilon \qquad (5)$$

The electron energy distribution is obtained from

$$\rho(\varepsilon) = \rho_v(E - E_b - \varepsilon)(L_{\max} + 1)^2 \qquad (6)$$

where

$$L_{\max} = b/\lambda\!\!\!^{-} \qquad (7)$$

Table 2. Autodetachment Rates and Lifetimes Calculated Using Klots' Microcanonical Rate Expression at Three Excitation Energies for $I^-(H_2O)_5$ and $I^-(CH_3OH)_7$

	ADE (eV)			calculated		observed
species	initial state	excited state (E_b)	pump (eV)	$k(E)$ (1/ps)	lifetime (ps)	lifetime (ps)
$I^-(H_2O)_5$	4.30	0.3	4.57	8.97×10^{-3}	111.50	59.4 ± 2.2
			4.71	3.93×10^{-2}	25.43	53.6 ± 1.9
			4.87	1.24×10^{-1}	8.04	23.2 ± 0.3
		0.22	4.57	5.92×10^{-2}	16.88	59.4 ± 2.2
			4.71	1.87×10^{-1}	5.33	53.6 ± 1.9
			4.87	4.90×10^{-1}	2.04	23.2 ± 0.3
$I^-(CH_3OH)_7$	4.60	0.06	4.71	6.54×10^{-3}	152.98	19.6 ± 0.5
			4.87	1.82×10^{-1}	5.49	12.4 ± 0.5
			5.06	1.01E+00	0.99	10.9 ± 0.7
		0.04	4.71	5.28×10^{-2}	18.94	19.6 ± 0.5
			4.87	7.01×10^{-1}	1.43	12.4 ± 0.5
			5.06	2.65E+00	0.38	10.9 ± 0.7

in which $\rho_v(x)$ is the density of neutral states, λ is the de Broglie wavelength of the electron and neutral species, and b is the classical hard-sphere collision radius. $W(E, E_b)$ is then given by

$$W(E,E_b) = \int_0^{E-E_b} \rho_v(x)\{1 + 2[2\mu b^2(E - E_b - x)/\hbar^2]^{1/2} + [2\mu b^2(E - E_b - x)/\hbar^2]\}\mathrm{d}x \qquad (8)$$

where μ is the reduced mass (effectively the mass of the electron). An electron spin degeneracy factor of 2 should also be included. The expressions given above assume that the rotational energy level spacing is much smaller than the excess energy imparted to the system and that the transmission coefficient, $T(\lambda, L)$, or "sticking probability", is 1 for $L \leq L_{\max}$ and 0 for $L > L_{\max}$.

Let us consider $I^-(H_2O)_5$ and $I^-(MeOH)_7$ as specific examples. Figure 4 shows that the excess energy E is given by

$$E = h\nu - \mathrm{ADE}(I^-(\mathrm{ROH})_n) + E_b \qquad (9)$$

where $\mathrm{ADE}(I^-(\mathrm{ROH})_n)$ is the adiabatic detachment energy of the initial cluster anion. For $I^-(H_2O)_5$, this was obtained either by extrapolating the adiabatic detachment energies described by Serxner et al.[6] or by selecting the onset of the spectral feature in the photoelectron spectrum of Markovich et al.,[36] yielding 4.22 and 4.43 eV, respectively. Because the binding energy of the neutral iodine atom is quite weak[9,14,33,37] (and probably similar) in both the intermediate anion and final neutral state, we took E_b to be the ADE of $(H_2O)_5^-$, and estimated it as 0.22 eV from the onset of the photoelectron spectrum of this cluster.[34] We note that the extraction of adiabatic rather than vertical detachment energies from unstructured photoelectron spectra is subject to considerable uncertainty, but our goal here is only to come up with reasonable initial estimates for use in eq 4.

Iodide−methanol energetics can be similarly described. The difference in energy between the $I^-(CH_3OH)_n$ and $I\cdots(CH_3OH)_n$ states was taken as the ADE estimated from unpublished single-photon photoelectron spectra measured at 240 nm in our laboratory, giving 4.60 eV for $I^-(CH_3OH)_7$. Again, neglecting the weak binding of the iodine atom, ADEs of the bare methanol cluster anions could be used to estimate E_b, however, no such values exist in this size range.[15] Instead, a selection of values ranging from slightly positive to slightly negative energies was utilized to test the effect of E_b on the autodetachment rate.

The evaluation of eq 4 also requires vibrational frequencies for determination of the total number and density of states. For consistency, frequencies calculated for neutral $(H_2O)_5$ and $(CH_3OH)_7$ clusters were used for both the intermediate $(\mathrm{ROH})_n^-$ and final $(\mathrm{ROH})_n$ species, under the assumption that the highly averaged quantities in eq 4 are relatively insensitive to the presence of an excess electron. As it is unclear if the iodine atom leaves the cluster before autodetachment occurs, particularly for $I^-(CH_3OH)_n$ clusters, vibrational frequencies associated with the iodine atom were not included. The geometries for various $(H_2O)_5^-$ isomers calculated with density functional theory by Herbert and Head-Gordon[38] were used as starting points for calculation of the corresponding neutral geometries. Neutral geometries were optimized with the B3LYP[39,40] density functional and the 6-31(1+, 3+)G* basis set using the Q-Chem electronic structure programming suite.[38,41] Frequencies were calculated using MP2/6-311(2+, 3+)G**. This method and basis set combination was previously used for geometry optimization for benchmark VDE calculations for clusters in our size range of interest.[42] A cyclic methanol cluster geometry was generated based on the lowest energy structure proposed by Buck et al.[43] and was optimized with B3LYP/6-31(1+, 3+)G*; frequencies were also calculated with this method and basis set. Vibrational densities of states were obtained from the Beyer−Swinehart direct counting algorithm which calculates all possible combinations of energy partitioning among vibrational modes of a system of harmonic oscillators.[31,44] The value of b needed for calculation of the electron emission rate was estimated from optimized structures.

Autodetachment rates and lifetimes were calculated over a range of values for $\mathrm{ADE}(I^-(\mathrm{ROH})_n)$ and E_b to test the model's sensitivity to these parameters. The full set of results is presented in the Supporting Information. Because calculated lifetimes for $I^-(H_2O)_5$ were found to be relatively insensitive to cluster geometry, the results displayed are those for a representative structure. Table 2 lists the energetics that lie within about an

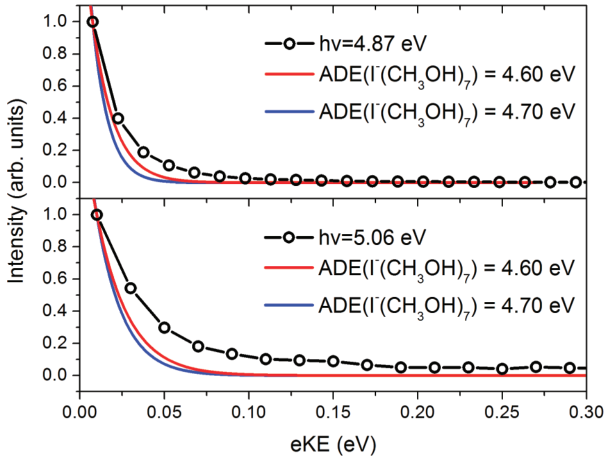

Figure 5. Simulated and experimental photoelectron spectra for $I^-(CH_3OH)_7$ excited at 4.87 eV (upper panel) and 5.06 eV (lower panel).

order of magnitude of the experimental results for all excitation wavelengths. For $I^-(H_2O)_5$, using 4.30 eV for the initial cluster anion ADE and either 0.30 or 0.22 eV for E_b gave acceptable agreement with experiment. These numbers are close to the initial estimates obtained from previous experimental work as described above. For $I^-(CH_3OH)_7$, acceptable agreement was found for values of 4.60 and 0.04 eV for ADE($I^-(ROH)_n$) and E_b, respectively. The parameters displayed in Table 2 were biased toward giving slightly faster rather than slower autodetachment compared to experiment as the calculations neglected effects due to anharmonicity of the vibrational modes that would be expected to increase the density of states and thus slow autodetachment.[30]

The results in Table 2 and the SI show that, as expected, eq 4 always yields lifetimes that decrease with increasing excitation energy, however in general calculated lifetimes changed more steeply with excitation energy than did measured lifetimes. Though changing either ADE value notably changes autodetachment lifetimes, we found that increasing E_b has a much greater effect than increasing ADE($I^-(ROH)_n$) by the same amount, that is, that the energy difference between the neutral and excited anion states is more important than the energy difference between the neutral and initial states. This trend is consistent with the greater stability of water cluster anions compared to small-chain alcohol cluster anions leading to lower electron emission rates for water-containing clusters. Interestingly, we found that even slightly negative values of E_b gave autodetachment lifetimes that were orders of magnitude larger than the experimental values. Whether this means that weakly bound bare methanol cluster anions in this size-range can exist remains open to investigation; as of yet, none have been seen in mass spectra of clusters from our ion source.[15]

We can also calculate the electron kinetic energy distribution from autodetachment, $\rho(\varepsilon)$, using eq 6. Examining eq 6, it is apparent that the choices of $E - E_b$ and L_{max} are the only parameters used to model the autodetachment spectral feature. As expressed in eq 9, the value of $E - E_b$ is equivalent to the difference between the excitation energy and the ADE of the initial state, so changing either value should simply shift the simulated curve for a constant L_{max}, altering the curvature of the normalized distribution in the energy range of interest. Calculations were performed assuming exclusively *s*-wave electron emission ($L_{max} = 0$). The assumption of *s*-wave emission is consistent with the isotropic ($\beta_2 \sim 0$) photoelectron angular distribution of the autodetachment feature (Figure 1); note that *s*-wave detachment does not involve a centrifugal barrier[45] and thus is expected to dominate for the low energy electrons associated with autodetachment in these experiments.

Simulated and measured spectra for $I^-(CH_3OH)_7$ excited with two different photon energies are shown in Figure 5. The simulated traces follow the shape of the autodetachment spectra reasonably well, though in both examples the curvature appears too shallow for eKE values near zero. This discrepancy may in part result from the neglect of anharmonicity in density of states calculations, which, while simplifying, should result in the increasingly significant underestimation of the neutral and, most prominently, anion density of states with increasing excess energy.[30]

The analysis outlined herein demonstrates that the microcanonical thermionic emission model put forth by Klots can reproduce the trends in our autodetachment rates for $I^-(ROH)_n$ clusters involving two different solvents as well as the electron kinetic energy distribution from autodetachment. This agreement is obtained using reasonable energetics for the quantities in Figure 4. It thus appears that our conceptual view of the autodetachment process as outlined in eq 3 is qualitatively correct, as is the idea that small variations in energetics have a significant effect on the autodetachment rate, thus explaining the slower autodetachment from $I^-(H_2O)_n$ clusters relative to comparably sized $I^-(CH_3OH)_n$ and $I^-(CH_3CH_2OH)_n$ clusters. On the other hand, more sophisticated treatments including anharmonicity are needed to improve agreement between calculated and measured autodetachment rates. The neglect of anharmonicity may be particularly important in the clusters containing methanol and ethanol because the resulting increase in the density of states will have to be compensated to some extent by reducing E_b, possibly yielding a negative value that would be more consistent with the non-observation of bare cluster anions in this size regime.

■ SUMMARY

Femtosecond time-resolved photoelectron imaging has been used to study the charge-transfer-to-solvent process of iodide-doped water and alcohol clusters as a function of excitation energy. $I^-(\text{ethanol})_n$ ($4 \leq n \leq 10$) clusters were also studied for the first time. The autodetachment decay channel was observed to deplete the CTTS excited state within 1−71 ps for iodide-doped methanol and ethanol clusters with 263 nm excitation while water-containing clusters were significantly more stable with respect to autodetachment due to the enhanced stability of bare water cluster anions compared to alcohol cluster anions. The similarity between iodide−methanol and iodide−ethanol cluster lifetimes with the same number of molecules alluded to an insensitivity to the quantity of vibrational modes in the system and provided further support for the idea that energetics are the driving factors for electron emission rates. The CTTS state for all systems studied was decreasingly stable to autodetachment as the excitation energy was increased from 4.57 to 5.06 eV as expected for a statistical process. Autodetachment lifetimes for $I^-(H_2O)_5$ and $I^-(CH_3OH)_7$ were modeled according to Klots' expressions for thermionic emission from clusters and the results found to qualitatively reproduce the trend of decreasing lifetime with increasing energy as well as the large discrepancy in length between the two solvents' lifetimes with reasonable energy parametrization. The quantitative difference between calculated and experimentally observed lifetimes likely results in part from the neglect of anharmonicity in density of states calculations and also from uncertainties in the energetics used to describe the system.

ASSOCIATED CONTENT

Supporting Information. Tables including additional calculated lifetimes for $I^-(H_2O)_5$ and $I^-(CH_3OH)_7$. This material is available free of charge via the Internet at http://pubs.acs.org.

AUTHOR INFORMATION

Corresponding Author

*E-mail: dneumark@berkeley.edu.

ACKNOWLEDGMENT

This work was supported by the National Science Foundation (NSF) under Grant CHE-0649647. M.A.Y. acknowledges funding from a National Defense Science and Engineering Graduate (NDSEG) Fellowship through the Air Force Office of Scientific Research (AFOSR), 32 CFR 168a. S.B.K. is grateful for funding through an NSF Graduate Research Fellowship.

REFERENCES

(1) Haranczyk, M.; Gutowski, M.; Li, X.; Bowen, K. H. *Proc. Natl. Acad. Sci. U.S.A.* **2007**, *104*, 4804.

(2) Simons, J. *Acc. Chem. Res.* **2006**, *39*, 772.

(3) Coe, J. V.; Lee, G. H.; Eaton, J. G.; Arnold, S. T.; Sarkas, H. W.; Bowen, K. H.; Ludewigt, C.; Haberland, H.; Worsnop, D. R. *J. Chem. Phys.* **1990**, *92*, 3980.

(4) Hammer, N. I.; Shin, J. W.; Headrick, J. M.; Diken, E. G.; Roscioli, J. R.; Weddle, G. H.; Johnson, M. A. *Science* **2004**, *306*, 675.

(5) Neumark, D. M. *Mol. Phys.* **2008**, *106*, 2183.

(6) Serxner, D.; Dessent, C. E. H.; Johnson, M. A. *J. Chem. Phys.* **1996**, *105*, 7231.

(7) Chen, X. Y.; Bradforth, S. E. *Annu. Rev. Phys. Chem.* **2008**, *59*, 203.

(8) Verlet, J. R. R.; Kammrath, A.; Griffin, G. B.; Neumark, D. M. *J. Chem. Phys.* **2005**, *123*, 4.

(9) Kammrath, A.; Verlet, J. R. R.; Bragg, A. E.; Griffin, G. B.; Neumark, D. M. *J. Phys. Chem. A* **2005**, *109*, 11475.

(10) Young, R. M.; Yandell, M. A.; Neumark, D. M. *J. Chem. Phys.* **2011**, *134*, 124311.

(11) Frischkorn, C.; Zanni, M. T.; Davis, A. V.; Neumark, D. M. *Faraday Discuss.* **2000**, *115*, 49.

(12) Zanni, M. T.; Frischkorn, C.; Davis, A. V.; Neumark, D. M. *J. Phys. Chem. A* **2000**, *104*, 2527.

(13) Ehrler, O. T.; Griffin, G. B.; Young, R. M.; Neumark, D. M. *J. Phys. Chem. B* **2009**, *113*, 4031.

(14) Chen, H. Y.; Sheu, W. S. *Chem. Phys. Lett.* **2001**, *335*, 475.

(15) Kammrath, A.; Verlet, J. R. R.; Griffin, G. B.; Neumark, D. M. *J. Chem. Phys.* **2006**, *125*, 4.

(16) Fox, M. F.; Hayon, E. *Chem. Phys. Lett.* **1974**, *25*, 511.

(17) Fox, M. F.; Hayon, E. *J. Chem. Soc., Faraday Trans. I* **1976**, *72*, 1990.

(18) Blandamer, M. J.; Fox, M. F. *Chem. Rev.* **1970**, *70*, 59.

(19) Klots, C. E. *Chem. Phys. Lett.* **1991**, *186*, 73.

(20) Davis, A. V.; Wester, R.; Bragg, A. E.; Neumark, D. M. *J. Chem. Phys.* **2003**, *118*, 999.

(21) Bragg, A. E.; Verlet, J. R. R.; Kammrath, A.; Cheshnovsky, O.; Neumark, D. M. *J. Am. Chem. Soc.* **2005**, *127*, 15283.

(22) Even, U.; Jortner, J.; Noy, D.; Lavie, N.; Cossart-Magos, C. *J. Chem. Phys.* **2000**, *112*, 8068.

(23) Wiley, W. C.; McLaren, I. H. *Rev. Sci. Instrum.* **1955**, *26*, 1150.

(24) Eppink, A.; Parker, D. H. *Rev. Sci. Instrum.* **1997**, *68*, 3477.

(25) Dribinski, V.; Ossadtchi, A.; Mandelshtam, V. A.; Reisler, H. *Rev. Sci. Instrum.* **2002**, *73*, 2634.

(26) Reid, K. L. *Annu. Rev. Phys. Chem.* **2003**, *54*, 397.

(27) Cooper, J.; Zare, R. N. *J. Chem. Phys.* **1968**, *48*, 942.

(28) Andersen, J. U.; Bonderup, E.; Hansen, K. *J. Phys. B: At. Mol. Opt. Phys.* **2002**, *35*, R1.

(29) Wurz, P.; Lykke, K. R. *J. Phys. Chem.* **1992**, *96*, 10129.

(30) Zhao, Y. X.; deBeer, E.; Xu, C. S.; Taylor, T.; Neumark, D. M. *J. Chem. Phys.* **1996**, *105*, 4905.

(31) Gilbert, R. G., Smith, S. C. *Theory of Unimolecular and Recominbation Reactions*; Blackwell Scientific Publications: Oxford, 1990.

(32) Lee, H. M.; Kim, D.; Kim, K. S. *J. Chem. Phys.* **2002**, *116*, 5509.

(33) Lee, H. M.; Suh, S. B.; Kim, K. S. *J. Chem. Phys.* **2003**, *119*, 7685.

(34) Kim, J.; Becker, I.; Cheshnovsky, O.; Johnson, M. A. *Chem. Phys. Lett.* **1998**, *297*, 90.

(35) Haberland, H.; Langosch, H.; Schindler, H. G.; Worsnop, D. R. *J. Phys. Chem.* **1984**, *88*, 3903.

(36) Markovich, G.; Pollack, S.; Giniger, R.; Cheshnovsky, O. *J. Chem. Phys.* **1994**, *101*, 9344.

(37) Lee, H. M.; Kim, K. S. *Mol. Phys.* **2004**, *102*, 2485.

(38) Herbert, J. M.; Head-Gordon, M. *Phys. Chem. Chem. Phys.* **2006**, *8*, 68.

(39) Becke, A. D. *J. Chem. Phys.* **1993**, *98*, 5648.

(40) Stephens, P. J.; Devlin, F. J.; Chabalowski, C. F.; Frisch, M. J. *J. Phys. Chem.* **1994**, *98*, 11623.

(41) Shao, Y.; Jung, L. F.-M.; Kussmann, J.; Ochsenfeld, C.; Brown, S. T.; Gilbert, A. T. B.; Slipchenko, L. V.; Levchenko, S. V.; O'Neill, D. P.; Distasio, R. A., Jr.; Lochan, R. C.; et al. *Phys. Chem. Chem. Phys.* **2006**, *8*, 3172.

(42) Herbert, J. M.; Head-Gordon, M. *J. Phys. Chem. A* **2005**, *109*, 5217.

(43) Buck, U.; Siebers, J. G.; Wheatley, R. J. *J. Chem. Phys.* **1998**, *108*, 20.

(44) Beyer, T.; Swinehart, D. F. *Commun. Assoc. Comput. Machines* **1973**, *16*, 379.

(45) Sadeghpour, H. R.; Bohn, J. L.; Cavagnero, M. J.; Esry, B. D.; Fabrikant, I. I.; Macek, J. H.; Rau, A. R. P. *J. Phys. B: At. Mol. Opt. Phys.* **2000**, *33*, R93.